C. R. Chimie 19 (2016) 909–920

Contents lists available at ScienceDirect

Comptes Rendus Chimie

www.sciencedirect.com

Full paper/Mémoire

Structural, physicochemical and in vitro pharmacological properties of the stimulant drug 8-chlorotheophylline complexed with Cr(III), Mn(II), Co(II), and Ni(II) metal ions: Potent metallodrug complexes as antimicrobial agents

Abdel Majid A. Adam

Department of Chemistry, Faculty of Science, Taif University, Al-Haweiah, P.O. Box 888, Zip Code 21974, Taif, Saudi Arabia

ARTICLE INFO

Article history:
Received 5 January 2016
Accepted 12 May 2016
Available online 28 June 2016

Keywords:
8-Chlorotheophylline
Metal complexes
Thermal decomposition
Biological activity

ABSTRACT

The interactions of methylxanthine bases with metal ions are of major biological interest and are important in bioinorganic chemistry. One of these bases is 8-chlorotheophylline (Ctp), which exhibits high stimulant action. Here, the metal complexation reactions of Ctp with Cr(III), Mn(II), Co(II), Ni(II), and Cu(II) ions were investigated, in a 1:2 molar ratio and in basic media. All of the prepared complexes were confirmed using elemental analysis, magnetic moment measurements, molar conductance, thermal analysis, and UV–Vis., IR, and Raman spectroscopies. Spectroscopic results revealed direct cation interactions for all of the metal ions via the deprotonated N7 atom of Ctp. The biological activity of the complexes was examined to determine the effect of chelation on the bioactivity of Ctp. It was observed that free Ctp possesses very low inhibitory activity towards several bacteria and fungi. However, the potency of its Cr(III)-complex exceeded that of the standard drug Ciprofloxacin against all of the tested bacterial strains, and the potency of this complex was 28% and 11% higher than those of the standard drug Fluconazole against the *Aspergillus flavus* and *Penicillium Sp* fungal strains, respectively.

1. Introduction

The increasing concern about antibiotic resistance caused by the clinical use of antibiotics or the occurrence and fate of antibiotic residues in the environment has motivated researchers to discover more effective drugs with the potential to extend over the antibacterial/antifungal spectrum and to overcome drug resistance. One promising class of compounds to achieve this goal is metallodrug compounds. The coordination chemistry of metallodrug compounds is attracting considerable interest from chemists and pharmacists, owing to their wide application in many fields, particularly in designing more biologically active drugs [1]. Several metallodrugs have been proven to possess interesting pharmaceutical properties such as antimicrobial, antiviral, and anticancer activity, and have been extensively used as antimicrobial chemotherapeutics [2–6].

Transition metal ions have an essential role in the field of medicinal biochemistry [7–10]. Transition metal complexes have been utilized as drugs and therapeutic agents to treat several human diseases such as carcinomas, lymphomas, infections, inflammation, diabetes, and neurological disorders [7,8]. Transition metals exhibit different oxidation states and can interact with a number of metal-binding sites. These properties of transition metals have led to the development of metal-based drugs with promising pharmacological applications, which may offer unique therapeutic opportunities [11]. The mode of action

E-mail address: majidadam@yahoo.com.

http://dx.doi.org/10.1016/j.crci.2016.05.010
1631-0748/

of metal complexes on living organisms is different from that of purely organic drugs. These complexes show great diversity in action [12]. This has, for instance, led to clinical applications as chemotherapeutic agents for cancer treatment, such as cisplatin [13].

Purine nucleobases are excellent ligands for metal ions [14]. Their interactions with metal ions are of major biological interest and are gaining importance in bioinorganic chemistry due to their effects on the stability, conformation, replication, and transcription of DNA [15]. Purines, such as caffeine, 8-chlorocaffeine, theophylline, and 8-chlorotheophylline (Scheme 1), are methylxanthine bases that are structurally related and have similar physiological effects. The metal complexes of caffeine and theophylline have been extensively reported to compare the binding of metal ions at the purine N7 and O6 sites. Caffeine has a CH_3 group at the N7 site that blocks the interaction of metal cations with the N7 atom, whereas in theophylline, the N7 site is accessible for metal ion coordination [16]. However, there are few reports in the literature on the metal complexes of 8-chlorotheophylline (Ctp). The most recent one by J. Deng et al., 2008 [17], reports the crystallographic structure of Ctp with Cu(II) ions. They concluded that the complex has the Cu atom at the center of a slightly distorted trans-square planar geometry coordinated by two deprotonated N atoms and two O atoms of water molecules. Ctp is a stimulant drug with physiological effects similar to those of caffeine and theophylline. It possesses several pharmacological properties and produces a number of effects, including nervousness, restlessness, insomnia, convulsions, anxiety, headaches, and nausea [18–20]. This work aimed to obtain several metal complexes containing Ctp and to investigate their biological properties. The objectives of the present work were as follows:

- Synthesis of metal–Ctp complexes with different metal ions (i.e. Cr(III), Mn(II), Co(II), Ni(II) and Cu(II)),with a 1:2 molar ratio. The complexation was carried out in a 1:1 methanol–water mixture in basic media using KOH.
- Characterization of the resultant products using elemental and spectroscopic data (UV–Vis., IR and Raman), molar conductance, and magnetic measurements.
- Comparative analysis of the thermal decomposition behavior of the complexes by thermogravimetry (TG/DTG and DTA).
- Assaying the antimicrobial activities of the complexes in vitro against two Gram-positive bacteria and two Gram-negative bacteria, as well as two fungi.

2. Results and discussion

2.1. Chemistry

2.1.1. CHN analysis results

All of the prepared complexes are colored, are stable in air, have high melting points (> 300 °C) and are insoluble in water and most organic solvents, except DMSO and DMF, with gentle heating. The elemental analyses of the complexes indicate a 1:2 metal-to-ligand stoichiometry for all complexes, and the results of the elemental analyses are consistent with the suggested formulas $Cr(Ctp)_2(Cl)(H_2O)_3]\cdot 5H_2O$, $[Mn(Ctp)_2(H_2O)_4]\cdot 2H_2O$, $[Co(Ctp)_2(H_2O)_4]\cdot H_2O$, $[Ni(Ctp)_2(H_2O)_2]$, and $[Cu(Ctp)_2(H_2O)_2]$.

2.1.2. Vibrational spectra

2.1.2.1. Vibrational modes of Ctp. The Ctp molecule has three coordination sites to bind metal ions: the N9, N7, and the carbonyl oxygen O6 atoms. Many studies [21–26] have confirmed that the N7 atom is the primary binding site and such binding is very common among purine–metal complexes. The IR absorption spectra of the free Ctp and the solid complexes were recorded in the wavenumber range 4000–400 cm^{-1} and are shown in Fig. 1S (Supplementary data). The free Ctp molecule shows characteristic absorption bands in the IR spectrum (Fig. 1S(A)): (*i*) *N–H vibrations*: the strong band observed at 3127 cm^{-1} is assigned to the N–H stretching vibration. (*ii*) *C=O vibrations*: the strong bands observed at 1714 and 1637 cm^{-1} are assigned to the ν_{as}(C=O) and ν_s(C=O) vibrations, respectively. (*iii*) *Ring vibrations* (*C–N, C=N, C=C vibrations*): the band observed at 1550 $cm^{-1}$is assigned to the C=N stretching mode. The band observed at 1449 $cm^{-1}$is assigned to the C=C stretching mode. The bands at 1276 and 1055 cm^{-1} are assigned to the ν_{as}(C–N) and ν_s(C–N) vibrations, respectively. (*iv*) *C–Cl vibrations*: the bands observed at 786 and 700 cm^{-1} may be assigned to ν_s(C–Cl). These assignments are in agreement with previously published data [27,28].

2.1.2.2. Vibrational modes of complexes. The reactions of Ctp with the metal ions were conducted in basic media (KOH in MeOH), so the Ctp molecule was deprotonated at the N7–H position [29]. This was confirmed by the absence, in all complexes, of the characteristic band resulting from the ν(N7–H) vibration occurring in free Ctp at 3127 cm^{-1}. None of the prepared complexes showed any absorbance assignable to the N7–H stretching vibrations in their IR spectra. Additionally, the two C=O (at positions 2 and 6)

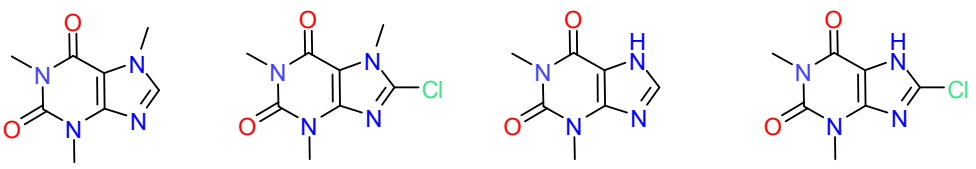

Scheme 1. Chemical structure of some methylxanthine bases.

stretching vibrations were found at approximately 1715–1709 cm^{-1} and 1639–1632 cm^{-1}, representing slight shifts relative to the analogous peaks at approximately 1714 and 1637 cm^{-1} in the free-Ctp spectrum. This indicates that the exocyclic oxygens at positions 2 and 6 did not form a bond with the metal center because coordination through one of these oxygens may cause a shift that would lower energy by approximately 40–50 cm^{-1} in the carbonyl vibration of the Ctp [30]. The bands assigned to the ν(C=N), ν_s(C–N), and ν_{as}(C–N) ring vibrations remained in the same position as observed in the free Ctp, indicating that C–N or C=N groups did not participate in the complexation. These observations suggest that the metal ion was bound to the same deprotonated N7 atom in all of the compounds. The broad bands observed between approximately 3390 and 3360 cm^{-1} are assigned to the ν(O–H) stretching vibrations of the coordinated or uncoordinated water molecules. The weak to very weak bands observed in the range 586–499 cm^{-1} could be assigned to the stretching vibration of the ν(M–N) band [31]. The bands observed at approximately 450 cm^{-1} in the Raman spectra of the complexes could be assigned to the ν(M–OH_2) vibration [24]. The Raman lines observed at 362 and 310 cm^{-1} in the spectrum of the Cr(III) complex are assigned to the ν(M–Cl) vibration [24].

2.1.3. Molar conductance and magnetic measurements

Table 1S lists the molar conductance and magnetic moment values of free Ctp and its metal complexes using 10^{-3} M solutions in DMSO at 25 °C. The metal complexes are found to have molar conductance values of 31–70 Ω^{-1} cm^2 mol^{-1} indicating a slightly conductive nature [32,33]. The value of the molar conductance of the Cr(III) complex is higher compared to the corresponding values of the other complexes. The presence of chloride ions inside or outside the coordination sphere was confirmed by the silver nitrate test. The effective magnetic moment (μ_{eff}) value was obtained using the equations described in the Supplementary data [34]. The values of μ_{eff} indicate a paramagnetic character with six-coordinate chelation modes for Cr(III), Mn(II), and Co(II) ions, and four-coordinate chelation modes for Ni(II) and Cu(II) ions. The μ_{eff} values of the Cr(III), Mn(II), and Co(II) [35] complexes are found to be 3.82, 8.13, and 5.7 B.M., respectively, suggesting that they possess an octahedral configuration. In case of the Ni(II) complex, the experimentally obtained μ_{eff} value is 4.0 B.M., and this is expected to diminish markedly with temperature. At room temperature, tetrahedral complexes always show a magnetic moment > 3.3 B.M, usually ranging between 3.4 and 3.9 B.M. The μ_{eff} value in the present study also lies near this range (4.0 B.M). Hence, it can be concluded that the nickel(II) complex has a tetrahedral geometry in the solid state [36,37]. The Cu(II) complex has a μ_{eff} value of 2.1 B.M., which indicates a square planar structure [38–40].

2.1.4. UV–Vis. spectra

The solid reflectance spectra of the prepared complexes are shown in Fig. 2S (Supplementary data) and summarized in Table 1. The spectrum of the Cr(III) complex exhibits transitions at 15,873 cm^{-1} and 24,390 cm^{-1}, assignable to the spin allowed d–d transitions, $^4A_{2g}(F) \rightarrow {}^4T_{2g}(F)$ (ν1) and $^4A_{2g}(F) \rightarrow {}^4T_{1g}(F)$ (ν2), respectively. The spectrum of the Cr(III) complex also shows a third transition at 37,037 cm^{-1}, which may be due to the $^4A_{2g}(F) \rightarrow {}^4T_{1g}(P)$ (ν3) d–d transition. However, this transition is obscured by intraligand and charge transfer bands. The positions of these bands suggest an octahedral configuration around the Cr(III) ion [41,42]. The spectrum of the Mn(II) complex displays three medium-intensity bands at 16,234, 18,726, and 20,243 cm^{-1}, which can be assigned to $^6A_{1g} \rightarrow {}^4T_{1g}(G)$, $^6A_{1g} \rightarrow {}^4T_{2g}(G)$, and $^6A_{1g} \rightarrow {}^4E_g(G)$, $^4A_{1g}(G)$, respectively, for a Mn(II) ion in a distorted octahedral environment [43,44]. Octahedral Co(II) complexes have a pink or reddish brown color, whereas most tetrahedral Co(II) complexes have an intense blue or green color. The prepared Co(II)-Ctp complex has a pink color, indicating that this complex has an octahedral geometry. Three bands were detected in its spectrum at 16,181, 22,222, and 28,169 cm^{-1}, which were assigned to the $^4T_{1g}(F) \rightarrow {}^4T_{2g}(F)$, $^4T_{1g}(F) \rightarrow {}^4A_{2g}(F)$, and $^4T_{1g}(F) \rightarrow {}^4T_{1g}(P)$ transitions, respectively [45]. Generally, the electronic spectra of Ni(II) complexes show only L–L* transitions and strong charge transfer bands tailing into the whole of the visible region. The d–d transitions in tetrahedral Ni(II) complexes have very small extinction coefficients, due to which it is very difficult to record them in solution [46]. The solid reflectance spectrum of the Cu(II) complexes exhibited two bands; an asymmetric broad band at 16,666 cm^{-1} and a more intense band at 22,222 cm^{-1}. The former band may be assigned to the $^2T_{2g} \rightarrow {}^2E_g$ transition, while the latter band may be assigned to the ligand-metal charge transfer transition. The band position suggests a square-planar geometry [47–49].

Table 1
Solid reflectance spectral bands (cm^{-1}) of the complexes.

Complex	Spectra data (cm^{-1})	Electronic transition	Proposed geometry
Cr(III)	15,873	$^4A_{2g}(F) \rightarrow {}^4T_{2g}(F)$	Octahedral
	24,390	$^4A_{2g}(F) \rightarrow {}^4T_{1g}(F)$	
	37,037	$^4A_{2g}(F) \rightarrow {}^4T_{1g}(P)$	
Mn(II)	16,340	$^6A_{1g} \rightarrow {}^4T_{1g}(G)$	Octahedral
	18,484	$^6A_{1g} \rightarrow {}^4T_{2g}(G)$	
	20,202	$^6A_{1g} \rightarrow {}^4E_g(G)$, $^4A_{1g}(G)$	
Co(II)	16,420	$^4T_{1g}(F) \rightarrow {}^4T_{2g}(F)$	Octahedral
	22,272	$^4T_{1g}(F) \rightarrow {}^4A_{2g}(F)$	
	28,249	$^4T_{1g}(F) \rightarrow {}^4T_{1g}(P)$	
Cu(II)	16,666	$^2T_{2g} \rightarrow {}^2E_g$	Square planar
	22,222	L → M band	

2.1.5. ESR spectra

The X-band electron spin resonance (ESR) spectrum was acquired for the Cu(II) complex in DMSO at room temperature, and the parameters were estimated. The ESR spectral data are listed in Table 2, and the spectrum is presented in Fig. 1. Kivelson and Neiman [50] have reported a $g_{||}$ value < 2.3 for a metal–ligand bond with covalent character and

Table 2
ESR spectral parameters of the Cu(II) complex.

ESR data	$g_\perp$	$g_{||}$
Value	1.8140	1.9654

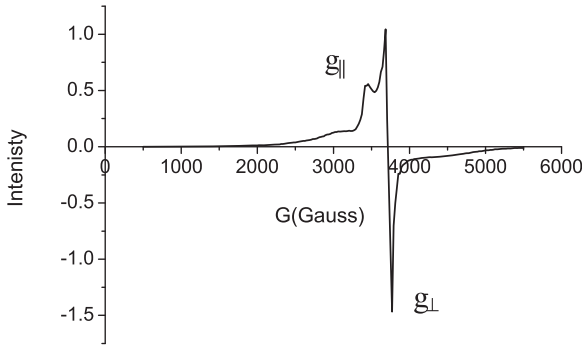

Fig. 1. The ESR spectrum of the Cu(II) complex at room temperature.

> 2.3 for ionic character. The value of $g_{||}$ for the Cu(II) complex is < 2.3, giving a clear assessment of the covalent character of the ligand-metal bond and the delocalization of the unpaired electrons [51]. The $g_{||}$ and $g_{\perp}$ values are 1.965 and 1.814, respectively, suggesting that a square planar structure exists around the Cu(II) ions [52].

2.2. Thermal characteristics

To confirm the compositions and structures of the formed complexes, thermal analyses (TG/DTG and DTA) were carried out for the free Ctp and its metal complexes. The measurements were carried out under a nitrogen atmosphere in the temperature range of 30–1000 °C. Their representative thermograms are illustrated in Fig. 2. The possible thermal degradation patterns for these compounds are collected in Table 3.

2.2.1. Thermogram properties

2.2.1.1. Free Ctp. The thermogram of free Ctp (Fig. 2A) indicates that it is thermally stable up to 225 °C, begins decomposing at ~225 °C and is completely decomposed at ~568 °C. Its thermal decomposition proceeds via two degradation steps. The first degradation step takes place in the temperature range of 30–339 °C, accompanied by an endothermic effect at 307 °C in the DTA response (306 °C; DTG) with an observed weight loss of 48.4%. The second step occurs within the temperature range of 339–568 °C, accompanied by a strong exothermic effect at 513 °C in the DTA with a weight loss of 51.6%.

2.2.1.2. Cr(III) complex. The Cr(III) complex is thermally decomposed in roughly two steps (Fig. 2B), within the temperature range of 95–413 °C. The release and pyrolysis of the 8-chlorotheophylline anion (Ctp^-) occur in the first decomposition step in the temperature range of 30–310 °C, along with the release of all of the coordinated and uncoordinated water molecules. This step is endothermic, with a maximum at 292 °C in DTA (294 °C; DTG) and with an observed weight loss of 45.89%. The pyrolysis of the second Ctp^- occurs in the temperature range of 310–413 °C and is accompanied on the DTA curve by one strong exothermic peak at 403 °C (400 °C; DTG), with an observed weight loss of 40.78% (cal. = 40.33%). The final decomposition product is Cr_2O_3 with some residual carbon.

2.2.1.3. Mn(II) complex. The thermogram of the Mn(II) complex indicates that it decomposes in three steps. The first decomposition step occurs in the temperature range of 30–183 °C, with two DTG_{max} of 110 and 167 °C corresponding to DTA_{max} of 114 and 176 °C, and has a weight loss of approximately 13.88% attributed to the loss of the $4.5H_2O$ molecules. The release and pyrolysis of the two Ctp^- begin and are completed in the next two steps. The first step occurs within the temperature range of 183–385 °C is accompanied on the DTA curve by an endothermic process with maxima at 333 and 370 °C. The second step occurs within the range of 385–576 °C and is accompanied by an exothermic process with maxima at 423 and 504 °C, leaving manganese (II) oxide (MnO) with some residual carbon as the final products.

2.2.1.4. Co(II) complex. The thermal degradation of the Co(II) complex exhibits four continuous steps in the temperature ranges of 30–195, 195–330, 330–438, and 438–572 °C, with DTA_{max} of 177 (endo), 288 (exo), 420 (exo), and 551 °C (exo), corresponding to weight losses of 12, 15.3, 22.94, and 36.2%, respectively. The thermogram shows that the first Ctp^- degrades in two steps in the temperature range of 195–438 °C, while the pyrolysis of the second Ctp^- (438–572 °C) occurs in one step, accompanied on the DTA curve by one strong exothermic peak at 551 °C (572 °C; DTG). Cobalt(II) oxide (CoO) is the final product, free of any residual carbon.

2.2.1.5. Ni(II) complex. The thermogram of the Ni(II) complex exhibits two steps and its thermal decomposition begins at 170 °C. The first degradation step occurs within the temperature range of 30–363 °C at DTG_{max} of 197 and 304 °C and DTA_{max} of 202 and 305 °C, corresponding to a weight loss of 42.98%. The second step occurs within the 363–570 °C temperature range (obs. = 36.87, cal. = 36.3%), accompanied by an exothermic effect with two maxima at 430 and 544 °C (DTA), leaving nickel (II) oxide (NiO) with some residual carbon as the final products.

2.2.1.6. Cu(II) complex. Thermoanalytical responses of the Cu(II) complex indicated that this compound is thermally stable up to 200 °C. Its decomposition occurred at three DTG_{max} of 251, 360, and 455 °C, corresponding to three DTA_{max} of 246 (endo), 371 (exo), and 467 °C (exo). The weight losses associated with these maximum temperatures were 27.4% (cal. = 27.26%), 55.45 (cal. = 55.33%), and 17.2% (cal. = 17.38%), respectively. CuO was the final product, with some residual carbon remaining stable up to 1000 °C as the final residues.

2.2.2. Comparison of the thermograms

The thermograms of the prepared complexes provided several observations. The Cr(III), Mn(II), Co(II), Ni(II), and Cu(II) complexes were stable up to ~95, 100, 110, 170, and 200 °C, respectively. The observed weight losses in each decomposition step were in agreement with the calculated weight losses. The complexes underwent several

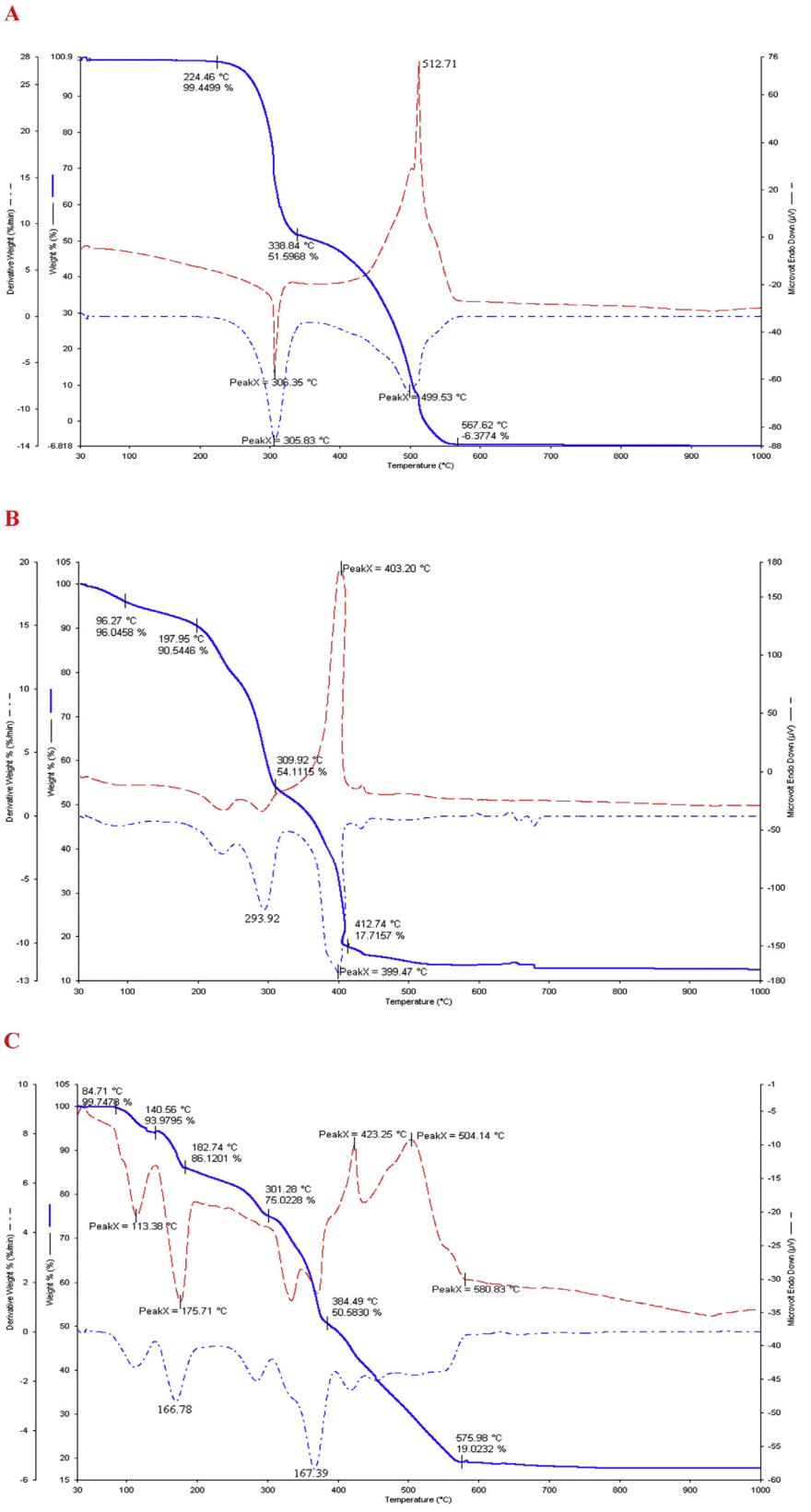

Fig. 2. TG, DTG and DTA thermograms of **A**; free Ctp and its metal complexes with **B**; Cr(III), **C**; Mn(II), **D**; Co(II), **E**; Ni(II), and **F**; Cu(II). (——) TG, (— · —) DTG and (— — —) DTA.

D

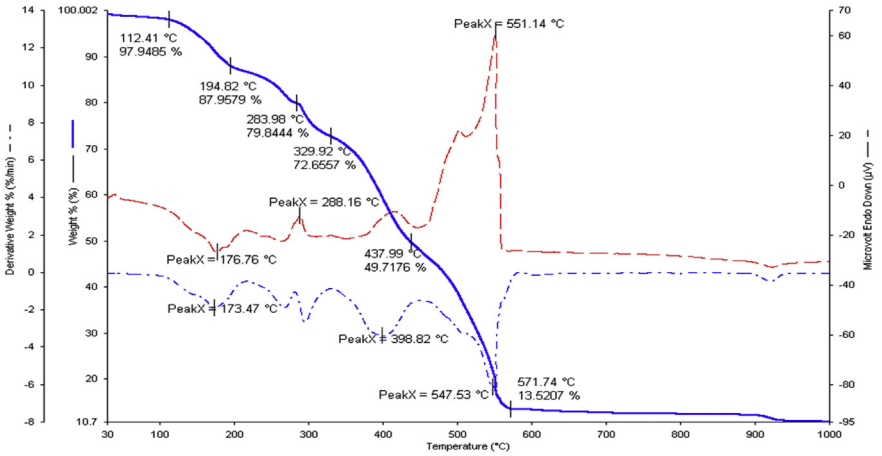

E

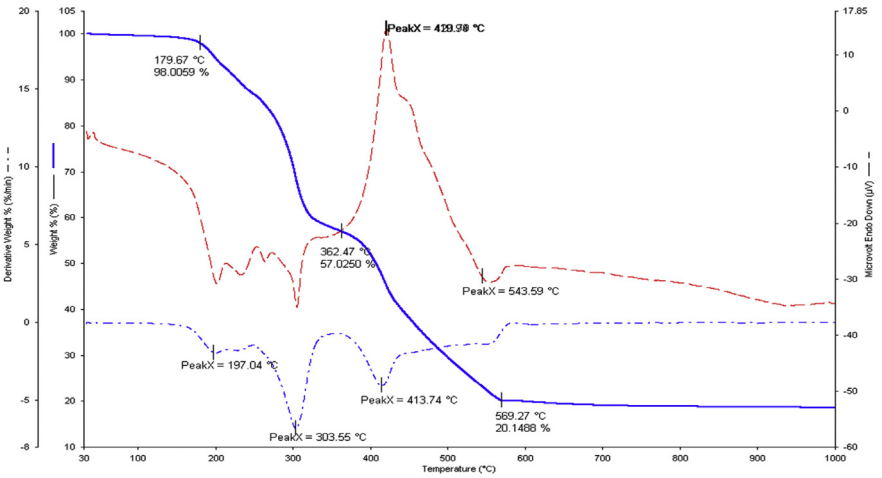

F

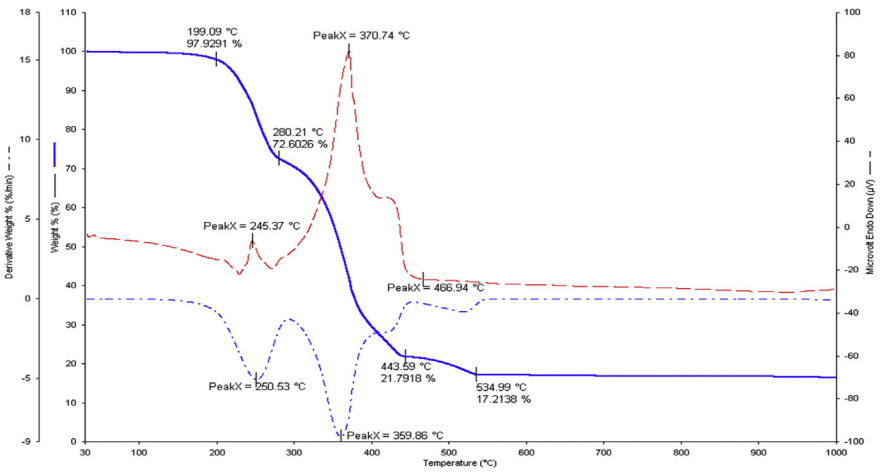

Fig. 2. (*continued*)

Table 3
Thermal decomposition data for the free Ctp and its metal complexes.

Compound		Stages	TG range (°C)	DTG max. (°C)	DTA max. (°C) (Endo↓, Exo↑)	TG% mass loss		Lost species
						Found	Calculated	
Ctp		I	30–339	306	307↓	48.40	48.67	$C_2H_2 + HCl + 1.5N_2$
		II	339–568	500	513↑	51.60	51.26	$2C_2H_2 + CO + NO$
Complexes	Cr(III)	I	30–310	230, 294	232↓, 292↓	45.89	46.29	$8H_2O + C_2H_2 + 1.75N_2 + ½NO + Cl_2$
		II	310–413	400	403↑	40.78	40.33	$2C_2H_2 + Ctp^-$
		Residue	–	–	–	13.33	13.36	$CrO_{1.5} + C$
	Mn(II)	I	30–183	110, 167	114↓, 176↓	13.88	13.73	$4.5H_2O$
		II	183–385	285, 368	333↓, 370↓	35.54	35.69	$1.5H_2O + 3C_2H_2 + 1.5N_2 + CO + ½Cl_2$
		III	385–576	418	423↑, 504↑	32.58	32.44	$2C_2H_2 + 1.5N_2 + 2NO + H_2 + ½Cl_2$
		Residue	–	–	–	18.00	18.12	$MnO + 3C$
	Co(II)	I	30–195	174	177↓	12.04	12.50	$4H_2O$
		II	195–330	285	288↑	15.30	15.27	$H_2O + N_2 + ½N_2 + CO$
		III	330–438	399	420↑	22.94	22.12	$3C_2H_2 + ½N_2 + ½Cl_2$
		IV	438–572	548	551↑	36.20	37.08	Ctp^-
		Residue	–	–	–	13.52	13.01	CoO
	Ni(II)	I	30–363	197, 304	202↓, 305↓	42.98	42.46	$2H_2O + 3C_2H_2 + 1.5N_2 + NO + ½Cl_2$
		II	363–570	414, 546	430↑, 544↑	36.87	36.30	$2C_2H_2 + 1.5N_2 + NO + CO + H_2 + ½Cl_2$
		Residue	–	–	–	20.15	21.21	$NiO + 3C$
	Cu(II)	I	30–280	251	246↓	27.40	27.26	$2H_2O + 1.5N_2 + NO + ½Cl_2$
		II	280–535	360, 455	371↑, 467↑	55.40	55.33	$6C_2H_2 + 1.5N_2 + CO + NO + ½Cl_2$
		Residue	–	–	–	17.20	17.38	$CuO + C$

decomposition steps resulting in metal oxides (Cr_2O_3, MnO, CoO, NiO and CuO) as the final decomposition products. Only the Co(II) complex showed almost complete decomposition of the ligand molecules without any carbon residue. The decomposition of the other complexes led to residual carbon atoms as a final product. Complexes of Cr(III), Ni(II), and Cu(II) ions were thermally decomposed in roughly two decomposition steps. The Mn(II) complex exhibited a three-stage degradation, while the Co(II) complex exhibited a four-stage degradation.

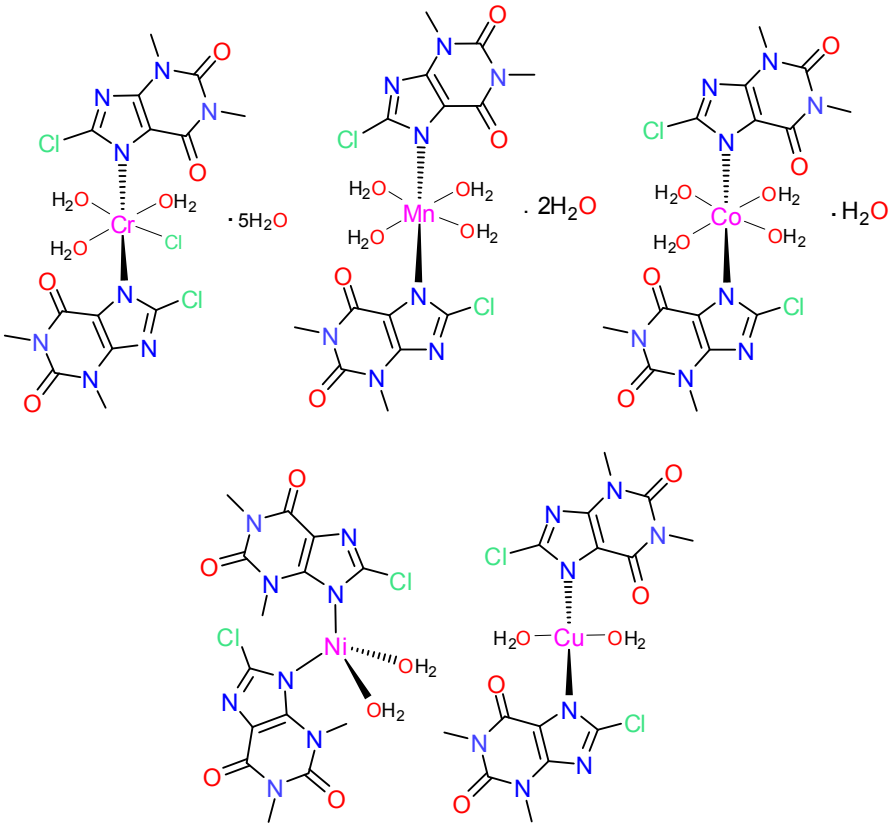

Scheme 2. Proposed structures of the Ctp-metal complexes.

Table 4
Antibacterial and antifungal activities of free Ctp, the metal salts and the prepared metal complexes.

Sample		Inhibition zone diameter in mm at 100 μg/ml					
		Bacterial strains				Fungal strains	
		Gram−positive strains		Gram−negative strains			
		S. aureus	*Bacillus subtilis*	*E. coli*	*P. aeruginosa*	*Aspergillus flavus*	*Penicillium Sp.*
DMSO (control)		0.0	0.0	0.0	0.0	0.0	0.0
Standards	Ciprofloxacin (Antibacterial agent)	23.0	25.0	19.0	20.0	–	–
	Fluconazole (Antifungal agent)	–	–	–	–	21.0	28.0
Free Ctp		0.0	4.0	1.0	3.0	3.0	6.0
Metal salts	$CrCl_3 \cdot 6H_2O$	10.0	10.0	11.0	13.0	11.0	9.0
	$MnCl_2 \cdot 4H_2O$	11.0	12.0	9.0	10.0	10.0	10.0
	$CoCl_2 \cdot 6H_2O$	13.0	13.0	10.0	11.0	12.0	12.0
	$NiCl_2 \cdot 6H_2O$	9.0	9.0	11.0	10.0	8.0	10.0
	$CuCl_2 \cdot H_2O$	13.0	13.0	12.0	12.0	9.0	10.0
Complexes	Cr(III)	25.0	26.0	22.0	23.0	27.0	31.0
	Mn(II)	20.0	28.0	19.0	19.0	19.0	24.0
	Co(II)	10.0	7.0	9.0	10.0	9.0	11.0
	Ni(II)	14.0	17.0	14.0	13.0	15.0	17.0
	Cu(II)	19.0	23.0	15.0	18.0	17.0	20.0

2.3. Complexation pathway

The characterization data are consistent with monodentate coordination of Ctp to metal ions through the deprotonated N7 atom, while the N9 and O6 atoms are not coordinated. Cr(III), Mn(II), and Co(II) ions form six-coordinate complexes while Ni(II) and Cu(II) form four-coordinate complexes. The suggested molecular formulae for the products consistent with these data are $Cr(Ctp)_2(Cl)(H_2O)_3]\cdot 5H_2O$, $[Mn(Ctp)_2(H_2O)_4]\cdot 2H_2O$, $[Co(Ctp)_2(H_2O)_4]\cdot H_2O$, $[Ni(Ctp)_2(H_2O)_2]$, and $[Cu(Ctp)_2(H_2O)_2]$ as described in Scheme 2.

2.4. Biology

The bioefficacy of free Ctp, metal salts, and prepared metal complexes was screened against the growth of various bacterial and fungal strains in vitro to evaluate their antimicrobial potential and to shed more light on the effect of complexation on drug activity. The screenings were performed with a 100 μg/mL concentration of the test compounds and an antibiotic disk. The zone diameters were measured to determine the effects on the growth of the tested microorganisms.

2.4.1. Antibacterial in vitro assessment

The antibacterial activity was screened in vitro against two Gram-positive bacterial strains (i.e. *Staphylococcus aureus* [*S. aureus*] and *Bacillus subtilis* [*B. subtilis*]) and two Gram-negative bacterial strains (i.e. *Escherichia coli* [*E. coli*] and *Pseudomonas aeruginosa* [*P. aeruginosa*]). Ciprofloxacin was employed as the standard drug (positive control) for comparison with the bacterial results. The results from the agar disk diffusion tests are presented in Table 4 and are statistically illustrated in Fig. 3.

The inhibition zone diameters of Ciprofloxacin (in mm) against *S. aureus*, *B. subtilis*, *E. coli*, and *P. aeruginosa* were found to be 23, 25, 19, and 20 mm, respectively. Under identical conditions, the corresponding values of the free

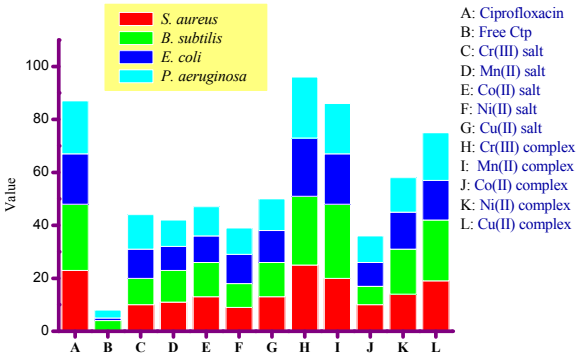

Fig. 3. Statistical representation for antibacterial activity of the standard drug, free Ctp, metal salts and metal complexes.

Ctp are 0, 4, 1, and 3 mm. Thus, free Ctp has very low inhibitory activity against all bacterial strains. The tested bacteria showed high resistance to free Ctp. The highest growth inhibition was induced by the Cr(III) and Mn(II)

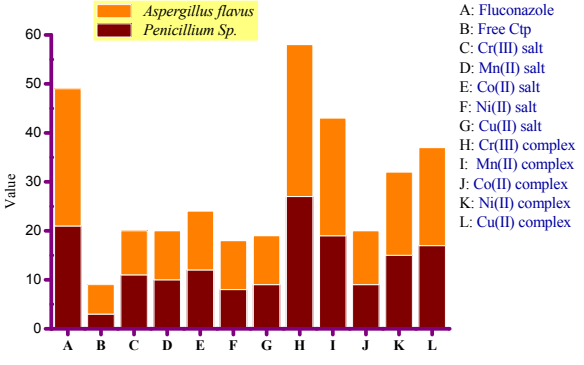

Fig. 4. Statistical representation for antifungal activity of the standard drug, free Ctp, metal salts and metal complexes.

complexes. The inhibition zone diameters of the Mn(II) complex were found to be 20, 28, 19, and 19 mm against *S. aureus*, *B. subtilis*, *E. coli*, and *P. aeruginosa*, respectively. These values were equipotent to the standard drug Ciprofloxacin; therefore, the Mn(II) complex displayed excellent toxicity towards the tested microorganisms. Under identical conditions, the corresponding values of the Cr(III) complex were 25, 26, 22, and 23 mm. From these values, it can be deduced that the potency of the Cr(III) complex exceeds that of the standard drug Ciprofloxacin against all strains, indicating that this complex possesses remarkable inhibitory activity against both types of bacteria, and thus may have broad-spectrum properties. The Ni(II) and Cu(II) complexes displayed good inhibitory results against the growth of the tested bacterial strains. The observed growth inhibitions by the Ni(II) complex are 14, 17, 14, and 13 mm, and the corresponding values of the Cu(II) complex are 19, 23, 15, and 18 mm against *S. aureus*, *B. subtilis*, *E. coli*, and *P. aeruginosa*, respectively. The Co(II) complex as well as the metal salts used in the preparation of metal complexes showed a similar degree of inhibition, and it ranged with 9–13 mm against the growth of the tested bacterial strains. free Ctp shows very low inhibition of the metabolic growth of both fungal strains. The inhibition zone diameters of the Cr(III) complex were found to be 27 and 31 mm against *A. flavus* and *Penicillium Sp*, respectively. These values indicate remarkable inhibitory activity of the Cr(III) complex against both fungal strains. The potency of this complex was greater than that of the standard drug Fluconazole by 28% and 11% against *A. flavus* and *Penicillium Sp*, respectively. The Mn(II), Ni(II), and Cu(II) complexes displayed strong antifungal response against the growth of fungal strains. The observed growth inhibitions of these three complexes were 19 and 24 mm for Mn(II) complex, 15 and 17 mm for Ni(II) complex, and 17 and 20 mm for Cu(II) complex against *A. flavus* and *Penicillium Sp*, respectively. The Co(II) complex and the metal salts used in the preparation of metal complexes showed a similar degree of inhibition, ranging from 8 to 12 mm against both fungal strains.

2.4.3. Activity index value

Antimicrobial activities of the complexes were confirmed by calculating the activity index (%) according to the following equation:

$$\text{Activity index}(\%) = \frac{\textit{Inhibition zone diameter of compound}\ (\text{mm})}{\textit{Inhibition zone diameter of standard drug}\ (\text{mm})} \times 100$$

2.4.2. Antifungal in vitro assessment

The free Ctp, metal salts, and prepared metal complexes were also examined for their antifungal properties against two fungal species, *Aspergillus flavus* and *Penicillium Sp*. The biological profiles of the antifungal results were compared with those of Fluconazole, which is a standard drug (positive control). The screening data are reported in Table 4 and are statistically represented in Fig. 4.

The inhibition zone diameters of fluconazole (in mm) against *A. flavus* and *Penicillium Sp* were found to be 21 and 28 mm, respectively. Under identical conditions, the corresponding values of the free Ctp were 3 and 6 mm. Thus, Table 5 lists the activity index values (%) of free Ctp and its metal complexes. The Cr(III) complex showed the highest activity indexes against all microbes compared with other complexes. The activity indexes of the complexes decrease in the following order: Cr(III) > Mn(II) > Cu(II) > Ni(II) > Co(II).

3. Conclusion

The aim of this work was to better understand the coordination behavior and biological properties of the drug Ctp with several metal ions (Cr(III), Mn(II), Co(II), Ni(II), and

Table 5
Activity index (%) for antimicrobial assay of free Ctp, the metal salts and the prepared metal complexes.

Sample		Activity Index (%)					
		Bacteria strains				Fungi strains	
		Gram–positive strains		Gram–negative strains			
		S. aureus	*Bacillus subtilis*	*E. coli*	*P. aeruginosa*	*Aspergillus flavus*	*Penicillium Sp.*
Free Ctp		0.0	16	5.3	15	14.3	21.4
Metal salts	$CrCl_3 \cdot 6H_2O$	43.5	40	57.9	65	52.4	32
	$MnCl_2 \cdot 4H_2O$	47.8	48	47.4	50	47.6	35.7
	$CoCl_2 \cdot 6H_2O$	56.5	52	52.6	55	57.1	42.9
	$NiCl_2 \cdot 6H_2O$	39	36	57.9	50	38	35.7
	$CuCl_2 \cdot H_2O$	56.5	52	63.2	60	42.9	35.7
Complexes	Cr(III)	109	104	116	115	128.6	110.7
	Mn(II)	87	112	100	95	90.5	85.7
	Co(II)	43.5	28	47.4	50	42.9	39.3
	Ni(II)	61	68	73.7	65	71.4	60.7
	Cu(II)	82.6	92	79	90	81	71.4

Cu(II)) in basic media (KOH in MeOH). The metal complexes were prepared and isolated and their structures were established based on a range of physicochemical methods, such as electronic and vibrational spectroscopies, as well as elemental and thermal analyses. The antimicrobial activity of the complexes was assessed against two types of bacterial and fungal species. The results suggest that Ctp molecules are coordinated to the metal ions in a monodentate manner through the deprotonated N7 atom, while the N9 and O6 atoms are not coordinated. An octahedral geometry was assigned for the Cr(III), Mn(II), and Co(II) complexes, a tetrahedral geometry for the Ni(II) complex, and a square-planar configuration for the Cu(II) complex. The antimicrobial activities of the metal complexes markedly exceed those of the uncomplexed metal ions, especially for the Cr(III) and Mn(II) complexes.

4. Experiments

4.1. Chemicals

All chemicals used were of analytical grade and were used as purchased. 8-Chlorotheophylline (Ctp; $C_7H_7ClN_4O_2$; 214.61), chemically 8-chloro-1,3-dimethyl-7*H*-purine-2,6-dione, was obtained from Sigma–Aldrich (USA), and it was used as such without further purification. $CrCl_3 \cdot 6H_2O$, $MnCl_2 \cdot 4H_2O$, $CoCl_2 \cdot 6H_2O$, $NiCl_2 \cdot 6H_2O$, $CuCl_2 \cdot H_2O$ and KOH were purchased from BDH (UK) and used without modification. HPLC-grade methanol was purchased from Merck (Darmstadt, Germany).

4.2. Syntheses of metal complexes

In a similar procedure to that reported in the literature [26], metal complexes of Cr(III), Mn(II), Co(II), Ni(II), and Cu(II) ions with Ctp were prepared by refluxing the Ctp ligand (2 mmol) and KOH (2 mmol) with each metal chloride salt (1 mmol) in a 1:1 methanol–water mixture on a hotplate for ~1–2 h at ~70 °C. The mixtures were left undisturbed overnight until the solid products completely precipitated. The colored solid precipitates were isolated, filtered and washed with two portions of cold methanol and diethyl ether to obtain the pure product. The products were then collected and dried under vacuum for 48 h.

4.3. Physicochemical techniques

4.3.1. CHN and melting point measurements

Microanalyses (C, H, and N) were performed using a PerkinElmer 2400 series CHN elemental analyzer (USA). The metal and water contents were determined gravimetrically. A Stuart Scientific electrothermal melting point apparatus was used to measure the melting points in glass capillary tubes in degrees Celsius.

4.3.2. Molar conductivity and magnetic measurements

The molar conductance was measured on a HACH digital conductivity meter model using 10^{-3} M solutions in DMSO solvent. The mass susceptibility (X_g) was measured at room temperature using Gouy's method by a magnetic susceptibility balance from Johnson Matthey and Sherwood.

4.3.3. Spectrometers

The UV–Vis spectra were recorded over a wavelength range of 200–800 nm using a Jenway 6405 spectrophotometer with a 1 cm quartz cell. The infrared (IR) spectra of the solid products (as KBr discs) were acquired at room temperature using a Shimadzu FT-IR spectrophotometer (Japan) over the range of 4000–400 cm^{-1} with 30 scans at a 2 cm^{-1} resolution. The Raman spectra were acquired on a Bruker FT-Raman spectrophotometer (Germany) equipped with a 50 mW laser. The electron spin resonance (ESR) spectra were acquired at room temperature on a Jeol JES-FE2XG ESR-spectrometer, at a frequency of 9.44 GHz with a Jeol microwave unit.

4.3.4. Thermal measurements

Thermogravimetric analysis (TG), differential thermogravimetric analysis (DTG), and differential thermal analysis (DTA) measurements were conducted using a Shimadzu TGA–50H thermal analyzer (Japan) with standard platinum TG pans. The measurements were performed at a constant heating rate of 10 °C/min over the temperature range of 30–1000 °C in a nitrogen atmosphere using alumina powder as the reference material.

4.4. Characterization of the products

4.4.1. Free Ctp

White powder; mp, 290–292 °C. Anal. data, calculated for $C_7H_7ClN_4O_2$ (214.61), Calcd, %: C, 39.14; H, 3.26; N, 26.09; Cl: 16.52. Found, %: C, 39.17; H, 3.22; N, 26.15; Cl: 16.47. IR data (KBr, cm^{-1}): υ_{max} 3127 ν(N–H), 2994 and 2873 ν_s(C–H) + ν_{as}(C–H); CH_3, 1714 ν_{as}(C=O), 1637 ν_s(C=O), 1550 ν(C=N), 1449 ν(C=C), 1373 δ_{def}(C–H), 1276 ν_{as}(C–N), 1055 ν_s(C–N), 992 δ_{rock}; CH_3, 786 and 700 ν(C–Cl). Raman data (cm^{-1}): υ_{max} 3119 ν(N–H), 2955ν_s(C–H) + ν_{as}(C–H); CH_3, 1702 ν_{as}(C=O), 1614 ν_s(C=O), 1548ν(C=N), 1437ν(C=C), 1386 δ_{def}(C–H), 1223 ν_{as}(C–N), 1038 ν_s(C–N), 985 δ_{rock}; CH_3, 701 ν(C–Cl).

4.4.2. Cr(III) complex

Green powder; mp, > 300 °C. Anal. data, calculated for $C_{14}H_{30}Cl_3N_8O_{12}Cr$ (660.67), Calcd, %: C, 25.43; H, 4.54; N, 16.95; Cl: 16.1, Cr: 7.87. Found, %: C, 25.49; H, 4.57; N, 16.90; Cl: 15.94; Cr: 7.82. IR data (KBr, cm^{-1}): υ_{max} 3385 ν(O–H); H_2O, 2990 ν_s(C–H) + ν_{as}(C–H); CH_3, 1715 ν_{as}(C=O), 1639 ν_s(C=O), 1551ν(C=N), 1449 ν(C=C), 1374 δ_{def}(C–H), 1277 ν_{as}(C–N), 1056 ν_s(C–N), 983 δ_{rock}; CH_3, 780 and 701 ν(C–Cl), 499 ν(M–N). Raman data (cm^{-1}): υ_{max} 2943 ν_s(C–H) + ν_{as}(C–H); CH_3, 1700 ν_{as}(C=O), 1618ν_s(C=O), 1546 ν(C=N), 1440 ν(C=C), 1385 δ_{def}(C–H), 1225 ν_{as}(C–N), 1037 ν_s(C–N), 985 δ_{rock}; CH_3, 700 ν(C–Cl), 441 ν(M–OH_2), 362 and 310 ν(M–Cl).

4.4.3. Mn (II) complex

Light brown powder; mp, > 300 °C. Anal. data, calculated for $C_{14}H_{26}Cl_2N_8O_{10}$ Mn (592.16), Calcd, %: C, 28.37; H, 4.39; N, 18.91; Cl: 11.97, Mn: 9.28. Found, %: C, 28.33; H, 4.36; N, 18.86; Cl: 12.03; Mn: 9.33. IR data (KBr, cm^{-1}): υ_{max} 3386 ν(O–H); H_2O, 3046 and 2817 ν_s(C–H) + ν_{as}(C–H); CH_3, 1709 ν_{as}(C=O), 1635 ν_s(C=O), 1552 ν(C=N), 1451 ν(C=C), 1377 δ_{def}(C–H), 1275 ν_{as}(C–N), 1057 ν_s(C–N), 992 δ_{rock};

CH_3, 776 and 702 ν(C–Cl), 510 ν(M–N). Raman data (cm^{-1}): υ_{max} 3026 ν_s(C–H) + ν_{as}(C–H); CH_3, 1705 ν_{as}(C=O), 1622 ν_s(C=O), 1542 ν(C=N), 1434 ν(C=C), 1391 δ_{def}(C–H), 1230 ν_{as}(C–N), 1044 ν_s(C–N), 980 δ_{rock}; CH_3, 700 ν(C–Cl), 449 ν(M–OH_2).

4.4.4. Co (II) complex

Pink powder; mp, > 300 °C. Anal. data, calculated for $C_{14}H_{24}Cl_2N_8O_9Co$ (578.15), Calcd, %: C, 29.06; H, 4.15; N, 19.37; Cl: 12.26, Co: 10.19. Found, %: C, 29.02; H, 4.08; N, 19.40; Cl: 12.32; Co: 10.14. IR data (KBr, cm^{-1}): υ_{max} 3392 ν(O–H); H_2O, 2977 ν_s(C–H) + ν_{as}(C–H); CH_3, 1710ν_{as}(C=O), 1632 ν_s(C=O), 1553 ν(C=N), 1445 ν(C=C), 1369 δ_{def}(C–H), 1277 ν_{as}(C–N), 1051 ν_s(C–N), 987 δ_{rock}; CH_3, 793 and 705 ν(C–Cl), 586 ν(M–N). Raman data (cm^{-1}): υ_{max} 2951 ν_s(C–H) + ν_{as}(C–H); CH_3, 1709 ν_{as}(C=O), 1627 ν_s(C=O), 1559 ν(C=N), 1439 ν(C=C), 1384 δ_{def}(C–H), 1229 ν_{as}(C–N), 1051 ν_s(C–N), 986 δ_{rock}; CH_3, 699ν(C–Cl), 453 ν(M–OH_2).

4.4.5. Ni (II) complex

Light green powder; mp, > 300 °C. Anal. data, calculated for $C_{14}H_{18}Cl_2N_8O_6Ni$ (523.91), Calcd, %: C, 32.07; H, 3.44; N, 21.38; Cl: 13.53, Ni: 11.20. Found, %: C, 32.14; H, 3.48; N, 21.44; Cl: 13.47; Ni: 11.13. IR data (KBr, cm^{-1}): υ_{max} 3376 ν(O–H); H_2O, 3044 ν_s(C–H) + ν_{as}(C–H); CH_3, 1710 ν_{as}(C=O), 1639 ν_s(C=O), 1549 ν(C=N), 1442 ν(C=C), 1368 δ_{def}(C–H), 1275 ν_{as}(C–N), 1052 ν_s(C–N), 985 δ_{rock}; CH_3, 792 and 703 ν(C–Cl), 578 ν(M–N). Raman data (cm^{-1}): υ_{max} 3004 ν_s(C–H) + ν_{as}(C–H); CH_3, 1702 ν_{as}(C=O), 1625 ν_s(C=O), 1561 ν(C=N), 1435 ν(C=C), 1390 δ_{def}(C–H), 1234 ν_{as}(-C–N), 1050 ν_s(C–N), 979 δ_{rock}; CH_3, 702 ν(C–Cl), 450 ν(M–OH_2).

4.4.6. Cu (II) complex

Grey powder; mp, > 300 °C. Anal. data, calculated for $C_{14}H_{18}Cl_2N_8O_6Cu$ (528.77), Calcd, %: C, 31.77; H, 3.40; N, 21.18; Cl: 13.41, Cu: 12.02. Found, %: C, 31.71; H, 3.47; N, 21.15; Cl: 13.45; Cu: 11.96. IR data (KBr, cm^{-1}): υ_{max} 3359 ν(O–H); H_2O, 3051, 2956 and 2853 ν_s(C–H) + ν_{as}(C–H); CH_3, 1709 ν_{as}(C=O), 1632 ν_s(C=O), 1548 ν(C=N), 1449 ν(C=C), 1365 δ_{def}(C–H), 1276 ν_{as}(C–N), 1057 ν_s(C–N), 978 δ_{rock}; CH_3, 788 and 700 ν(C–Cl), 580 ν(M–N). Raman data (cm^{-1}): υ_{max} 3022 ν_s(C–H) + ν_{as}(C–H); CH_3, 1700 ν_{as}(C=O), 1633 ν_s(C=O), 1564 ν(C=N), 1438 ν(C=C), 1386 δ_{def} (C–H), 1230 ν_{as}(C–N), 1049 ν_s(C–N), 984 δ_{rock}; CH_3, 705 ν(C–Cl), 448 ν(M–OH_2).

4.5. Biological evaluation

4.5.1. In vitro antibacterial activity

The antibacterial activity of free Ctp, metal salts, the prepared complexes, and the pure solvent was tested in vitro using the modified Bauer–Kirby disc diffusion method [53]. The utilized test organisms were *S. aureus* (MSSA 22) and *B. subtilis* (ATCC 6051) as examples of Gram-positive bacteria and *E. coli* (K 12) and *P. aeruginosa* (MTCC 2488) as examples of Gram-negative bacteria. The experiments were conducted in the microanalysis facility at Cairo University, Egypt. Briefly, 100 μL of the test bacteria were grown in 10 mL fresh medium until they reached a count of approximately 10^8 cells/mL [54]. Then, a 100 μL microbial suspension was spread onto agar plates. The nutrient agar medium for the antibacterial tests consisted of 0.5% peptone, 0.1% beef extract, 0.2% yeast extract, 0.5% NaCl and 1.5% agar-agar [55]. Isolated colonies of each organism that may play a pathogenic role were selected from the primary agar plates and tested for susceptibility. After the plates were incubated for 48 h at 37 °C, the inhibition (sterile) zone diameters (including the disc) in mm were measured using slipping calipers from the National Committee for Clinical Laboratory Standards (NCCLS, 1993) [56]. The screening was performed using 100 μg/mL of the complex. An antibiotic disc containing Ciprofloxacin (Antibacterial agent, 30 μg/disc, Hi-Media) was employed as the positive control. A filter disk impregnated with 10 μL of solvent (distilled water, chloroform, and DMSO) was employed as the negative control.

4.5.2. In vitro antifungal activity

The free Ctp, metal salts and the prepared complexes were also screened for their antifungal property using the modified Bauer–Kirby disc diffusion method. The utilized test organisms were *A. flavus* (laboratory isolate) and *Penicillium Sp* [53]. The complexes were dissolved in DMSO. The medium for the antifungal tests consisted of 3% sucrose, 0.3% $NaNO_3$, 0.1% K_2HPO_4, 0.05% KCl, 0.001% $FeSO_4$, and 2% agar-agar [54]. The disc diffusion method followed the approved standard method (M38-A) [57] developed by the NCCLS for evaluating the susceptibility of filamentous fungi to antifungal agents. The disk diffusion method for yeast, which was developed as the standard method (M44-P) by the NCCLS, was employed [58]. The plates that were inoculated with filamentous fungi or yeast were incubated for 48 h at 25 °C or 30 °C, respectively. The antifungal activity of the complexes was compared with that of Fluconazole (30 μg/disc, Hi-Media), which was used as the standard antifungal agent (positive control). A filter disk impregnated with 10 μL of solvent (distilled water, chloroform, and DMSO) was employed as the negative control. The antifungal activity was determined by measuring the diameters of the sterile zone (mm) in triplicate.

Appendix A. Supplementary data

Supplementary data related to this article can be found at http://dx.doi.org/10.1016/j.crci.2016.05.010.

References

[1] E. Alessio, Bioinorganic Medicinal Chemistry, Wiley-VCH Verlag GmbH and Co. KGaA, 2011.
[2] F. Trudu, F. Amato, P. Vaňhara, T. Pivetta, E.M. Peña-Méndez, J. Havel, J. Appl. Biomed. 13 (2) (2015) 79.
[3] C. Crisóstomo-Lucas, P. García-Holley, S. Hernández-Ortega, F. Sánchez-Bartéz, I. Gracia-Mora, N. Barba-Behrens, Inorg. Chim. Acta 438 (2015) 245.
[4] U. Singh, A.M. Malla, I.A. Bhat, A. Ahmad, M.N. Bukhari, S. Bhat, S. Anayutullah, A.A. Hashmi, Microb. Pathog. 93 (2016) 172.
[5] L.H. Abdel-Rahman, R.M. El-Khatib, L.A.E. Nassr, A.M. Abu-Dief, I. Mohamed, A.S. Amin, Spectrochim. Acta A 117 (2014) 366.
[6] N.T. Abdel Ghani, A.M. Mansour, Inorg. Chim. Acta 373 (2011) 249.
[7] P.P. Netalkar, S.P. Netalkar, V.K. Revankar, Polyhedron 100 (2015) 215.
[8] M.A. Ragheb, M.A. Eldesouki, M.S. Mohamed, Spectrochim. Acta A 138 (2015) 585.

[9] M.S. Refat, S.A. El-Shazly, Eur. J. Med. Chem. 45 (7) (2010) 3070.
[10] S.M. El-Megharbel, R.Z. Hamza, M.S. Refat, Chem. Bio. Interact. 220 (2014) 169.
[11] S. Rafique, M. Idrees, A. Nasim, H. Akbar, A. Athar, Biotechnol. Mol. Biol. Rev. 5 (2) (2010) 38.
[12] K. Hariprasath, B. Deepthi, I.S. Babu, P. Venkatesh, S. Sharfudeen, V. Soumya, J. Chem. Pharm. Res. 2 (4) (2010) 496.
[13] C. Pieter, A. Bruijnincx, P.J. Sadler, Curr. Opin. Biol. 12 (2) (2008) 197.
[14] C.G.A. Persson, J. Aller, Clin. Immunol. 78 (1986) 780.
[15] A.G. Halpert, M.C. Olmstead, R.J. Beninger, Neurosci. Biobehav. Rev. 26 (2002) 61.
[16] R.D. Spealman, Psychopharmacology 95 (1988) 19.
[17] J. Deng, Z. Xiong, Y. Yi, L. Yuan, H. Guo, M. Guo, L. Liu, Acta Cryst. E 64 (2008) m1159–m1160.
[18] D. Brackemeyer, A. Hervé, C.S. Brinke, M.C. Jahnke, F.E. Hahn, J. Am. Chem. Soc. 136 (2014) 7841.
[19] S. Nafisi, M. Monajemi, S. Ebrahimi, J. Mol. Struct. 705 (2004) 35.
[20] A.T. Tu, J.A. Reinosa, Biochemistry 5 (1966) 3375.
[21] N.S. Begum, H. Manohar, Polyhedron 13 (2) (1994) 307.
[22] S.D. Rothenberger, M.S. Zitzman, W.J. Birdsall, J. Inorg. Nucl. Chem. 43 (1981) 1673.
[23] W.J. Birdsall, M.S. Zitzman, J. Inorg. Nucl. Chem. 41 (1978) 116.
[24] W.J. Birdsall, Inorg. Chim. Acta 99 (1985) 59.
[25] S. Nafisi, D.S. Shamloo, N. Mohajerani, A. Omidi, J. Mol. Struct. 608 (2002) 1.
[26] A. Romerosa, C. López-Magaña, M. Saoud, S. Mañas, E. Colacio, J. Suárez-Varela, Inorg. Chim. Acta 307 (2000) 125.
[27] A.R. Noms, R. Kumar, E. Buncel, A.L. Beauchamp, J. Inorg. Biochem. 21 (4) (1984) 277.
[28] A.M.A. Adam, M.S. Refat, J. Mol. Liq. 209 (2015) 33.
[29] D. Lichtenberg, F. Bergmann, Z. Neiman, J. Chem. Soc. C (1971) 1676.
[30] A.L. Abuhijleh, H.A. Ali, A. Emwas, J. Organomet. Chem. 694 (2009) 3590.
[31] K. Nakomoto, Infrared Spectra of Inorganic and Coordination Compounds, Willey, New York, 1970.
[32] W.J. Geary, Coord. Chem. 7 (1971) 81.
[33] M.S. Refat, M.Y. El-Sayed, A.M.A. Adam, J. Mol. Struct. 1038 (2013) 62.
[34] P.F. Selwood, Magnetochemistry, 2nd ed., Wiley (Interscience), NY, 1956.
[35] F.A. Cotton, D.M.L. Goodgame, M. Goodgame, J. Am. Chem. Soc. 83 (23) (1961) 4690.
[36] S. Chandra, K.B. Pandya, S.K. Sindhwani, R.P. Singh, Gazz. Chim. Ital. 110 (1980) 207.
[37] S. Chandra, L.K. Gupta, J. Indian Chem. Soc. 81 (2004) 833.
[38] A.B.P. Lever, Coord. Chem. Rev. 3 (1968) 119.
[39] A.B.P. Lever, Inorganic Electronic Spectroscopy, 2nd ed., Elsevier, Amsterdam, 1997.
[40] F.A. Cotton, G. Wilkinson, C.A. Murillo, M. Bochmann, Advanced Inorganic Chemistry, 6th ed., Wiley, New York, 1999.
[41] M.S. Refat, Spectrochim. Acta A 133 (2014) 281.
[42] A.K. Sharma, S. Chandra, Spectrochim. Acta A 78 (2011) 337.
[43] J.R. Allan, N.D. Baird, A.I. Kassyk, J. Therm. Anal. 16 (1979) 79.
[44] F.A. Al-Saif, M.S. Refat, J. Mol. Struct. 1021 (2012) 40.
[45] A.M.A. Alaghaz, H.A. Bayoumi, Y.A. Ammar, S.A. Aldhlmani, J. Mol. Struct. 1035 (2013) 383.
[46] L.K. Gupta, U. Bansal, S. Chandra, Spectrochim. Acta A 66 (2007) 972.
[47] J.B. Gandhi, N.D. Kulkarni, Transit. Met. Chem. 26 (2001) 96.
[48] Z.D. Matović, V.D. Miletić, G. Samardžć, G. Pelosi, S. Ianelli, S. Trifunović, Inorg. Chim. Acta 358 (2005) 3135.
[49] M.S. Refat, N.M. El-Metwaly, Spectrochim. Acta A 92 (2012) 336.
[50] D. Kivelson, R. Neiman, J. Chem. Phys. 35 (1961) 149.
[51] P. Tharmaraj, D. Kodimunthiri, C.D. Sheela, C.S.S. Priya, J. Serb. Chem. Soc. 74 (8–9) (2009) 927–938.
[52] M.S. Refat, Spectrochim. Acta A 68 (2007) 1393.
[53] A.W. Bauer, W.M. Kirby, C. Sherris, M. Turck, Am. J. Clin. Pathol. 45 (1966) 493.
[54] M.A. Pfaller, L. Burmeister, M.A. Bartlett, M.G. Rinaldi, J. Clin. Microbiol. 26 (1988) 1437.
[55] D.J. Beecher, A.C. Wong, Appl. Environ. Microbiol. 60 (1994) 4614.
[56] National Committee for Clinical Laboratory Standards, Methods for Antimicrobial Susceptibility Testing of Anaerobic Bacteria: Approved Standard M11-A3, NCCLS, Wayne, PA, USA, 1993.
[57] National Committee for Clinical Laboratory Standards, Reference Method for Broth Dilution Antifungal Susceptibility Testing of Conidium-Forming Filamentous Fungi: Proposed Standard M38-A, NCCLS, Wayne, PA, USA, 2002.
[58] National Committee for Clinical Laboratory Standards, Method for Antifungal Disk Diffusion Susceptibility Testing of Yeast: Proposed Guideline M44-P, NCCLS, Wayne, PA, USA, 2003.